Hindawi
Journal of Chemistry
Volume 2019, Article ID 5271923, 10 pages
https://doi.org/10.1155/2019/5271923

Research Article

Investigation of the Thermal Performance of Salt Hydrate Phase Change of Nanoparticle Slurry Flow in a Microchannel

Safi A. Memon,[1] **M. B. Sajid**,[2] **M. S. Malik**,[3] **Awad B. S. Alquaity**,[4] **M. Mohib ur. Rehman**,[3] **Taqi A. Cheema**,[3] **Moon Kyu Kwak**,[1] **and Cheol Woo Park**[1]

[1]*School of Mechanical Engineering, Kyungpook National University, 80 Daehakro, Bukgu, Daegu 41566, Republic of Korea*
[2]*U.S.-Pakistan Center for Advanced Studies in Energy (USPCAS-E), National University of Sciences and Technology (NUST), Sector H-12, Islamabad, Pakistan*
[3]*Faculty of Mechanical Engineering, Ghulam Ishaq Khan Institute of Engineering Sciences & Technology (GIKI), Topi, Pakistan*
[4]*Institute for Combustion Technology, RWTH Aachen University, Aachen 52056, Germany*

Correspondence should be addressed to Cheol Woo Park; chwoopark@knu.ac.kr

Received 15 October 2018; Accepted 4 December 2018; Published 3 January 2019

Guest Editor: Hakjin Kim

Computational study was conducted to investigate the thermal performance of water-based salt hydrate S44 nanoparticles as the phase change material (PCM) in a microchannel heat sink. Constant heat dissipation was applied on the top wall of the heat sink. Forced internal convection of the PCM slurry flow was performed through a homogeneous approach. Three thermal performance parameters, including effectiveness ratio, performance index, and Merit number, were used to quantify the cooling performance of S44 for various concentrations of the PCM nanoparticles. The thermal performance of the salt hydrate S44 slurry was also compared with a similar study conducted for lauric acid nanoparticle slurry found in the literature. Specific operating conditions were identified. The salt hydrate S44 would provide better thermal performance than lauric acid, and vice versa. Finally, Nusselt number correlations have been developed for the microchannel PCM heat sink for Reynolds numbers in the range 12.23 to 47.14 and Prandtl numbers in the range 3.74 to 5.30. A design guideline for manufacturing PCM particles and microchannel heat sinks is provided. With this guideline, the heat absorption ability of the heat sink is maximized, and the pumping power and the losses related to the addition of the particles are minimized.

1. Introduction

The miniaturization of electronic devices coupled with advances in microscale manufacturing technology has prompted studies on increased thermal management and cooling performance in microchannels. Several studies have aimed at solving different problems involving microchannel heat sinks. An emerging problem involving conventional microchannel heat sinks underscores their inability to meet the ever-increasing cooling requirement of modern microelectronic devices, which can easily reach 10^5 W/cm^3 [1]. Electronic devices must remain cool to reduce the logic gate switching time and improve the processing speeds. In an attempt to meet this challenge, phase change material (PCM) particles may be introduced in the fluid flow of microchannel heat sinks to increase their cooling capacity. PCM particles act as the thermal storage device by undergoing a solid-to-liquid phase transformation when exposed to heat flux, thereby absorbing a large amount of heat. When thermal energy is required, PCM may be solidified, thereby releasing a large amount of energy. The key factor affecting heat transfer when a slurry containing PCM particles is introduced inside the microchannel is PCM's latent heat of fusion. The particles keep absorbing a large amount of heat from the electronic device until they are fully melted. Therefore, introducing PCM slurry inside a microchannel heat sink reduces the temperature difference along the microchannel length and increases the overall heat transfer coefficient.

Research on thermal management using PCM has evolved over the past two decades, as shown by the following studies: Goel et al. [2], Roy and Sengupta [3], Alvarado et al. [4], Hao and Tao [5], Kuravi et al. [6], Sabbah et al. [7], Kuravi et al. [8], Kondle et al. [9], Xing et al. [1], Alquaity et al. [10–12], Stritih [13], Wang et al. [14], Saha and Dutta

[15], and Shatikian et al. [16]. The following studies have been conducted on the PCM micro- and nanoparticle applications in heat exchangers: Goel et al. [2], Roy and Sengupta [3], Alvarado et al. [4], and Hao and Tao [5]. Goel et al. [2] studied microencapsulated particles of *n*-eicosane in a fully developed slurry flow with laminar flow regime in a circular channel that possesses a circular cross section under constant heat flux and temperature at the boundaries. By using slurry instead of pure fluid, a decrease of 50% was observed in the wall temperature. Roy and Sengupta's experiments used four different combinations, which were formed using two microencapsulated PCMs and two wall thicknesses [3]. They studied stability of the PCM heat sinks in thermal and structural terms and concluded that usage of microencapsulated particles in heat sinks is suitable for practical purposes. Alvarado et al. [4] experimentally studied turbulent flow in a copper channel with circular cross section under constant heat flux. The author concluded that concentration significantly contributed to the thermal storage of the microencapsulated PCM particles. Hao and Tao [5] computationally investigated the hydrodynamic characteristics along with the heat transfer of PCM slurry with micro- and nanosized PCM particles. Inclusion of PCM particles resulted in increase of heat transfer in the wall region. The application of PCM to microchannels is motivated by the advancement in microelectronic devices, thereby increasing thermal dissipation requirements of these devices, as indicated in the following studies: Kuravi et al. [6], Sabbah et al. [7], Kuravi et al. [8], Kondle et al. [9], Xing et al. [1], and Alquaity et al. [10–12]. The experimental and computational analyses performed by Kuravi et al. [6] investigated water-based PCM slurry flow containing *n*-octadecane microencapsulated particles through manifold microchannels. Thermal performance decreased in comparison with single fluid flow. However, the performance improved compared with single fluid flow when the hydraulic diameter of the channels decreased, and PCM with higher thermal conductivity was used. Sabbah et al. [7] conducted a 3D computational study of the microchannel PCM heat sink with microencapsulated PCM particles. The thermophysical properties of the slurry were assumed to be temperature dependent, and the thermal resistance of the microchannel walls was considered. The authors concluded that the heat sinks containing PCM slurry resulted in lower and more uniform temperatures across an electronic component when compared with heat sinks containing pure water. Kuravi et al. [8] computationally obtained the velocity and temperature profiles due to nanoencapsulated PCM in a 3D homogenous model of the microchannel with fin effect and longitudinal conduction along the microchannel. Kondle et al. [9] analyzed hydrodynamically developed laminar water-based *n*-eicosane slurry flow in different circular and rectangular microchannels using homogeneous models for the PCM slurry and a latent heat model to determine the effects of the phase change of the PCM on the heat transfer of the microchannel heat sink. Xing et al. [1] investigated the thermal performance of phase change slurry in microchannels with circular cross section. Governing equations were solved for the liquid and solid phases, and the interactions among the PCM particles were considered. Maximum heat transfer across the microchannel PCM heat sink was found for ranges of heat flux and Reynolds numbers. Alquaity et al. [12] studied two computational models, namely, homogeneous and discrete phase models [17], to identify which one is more suitable for studying PCM slurry flow in microchannels. The discrete phase model incorrectly predicted the pressure drop when the concentration of PCM was increased; hence, the homogeneous model was used for further studies. Alquaity et al. [11] defined the Merit number to account for the irreversibility effects caused by heat transfer and fluid friction. Detailed parametric study was conducted in which the bottom plate heat flux, inlet mass flow rate, and PCM concentration were varied to evaluate the thermal performance of the PCM. Homogenous model was used to model the slurry flow, whereas the thermophysical properties of the bulk fluid were assumed to be constant. The authors concluded that an optimal ratio of heat flux to mass flow rate exists, for which the thermal performance of the heat sink is maximized. Many studies have determined Nusselt number correlations for PCM heat sinks, as follows: Stritih [13], Wang et al. [14], Saha and Dutta [15], and Shatikian et al. [16]. Stritih [13] studied the solidification and melting behaviors of finned paraffin-based PCM thermal storage unit and compared it with a similar unit without fins. The author obtained time-varying temperature distribution and developed Nusselt number correlations as a function of the Rayleigh number for both solidification and melting cases. Wang et al. [14] developed two empirical Nusselt number correlations for 4 mm diameter circular tubes by considering the laminar and turbulent flow of slurries containing 0% to 27.6% bromohexadecane by mass. The correlations predicted the Nusselt number with more than 90% accuracy. Saha and Dutta [15] computationally studied the cooling performance of thermal conductivity enhancers of plate-fin type in PCM heat sinks. The authors conducted in-depth parametric studies by varying the aspect ratio and heat flux associated with the flow channel to obtain thermal performance and Nusselt number correlations for the PCM heat sink. A single Nusselt number correlation was insufficient to account for all aspect ratios. Hence, the authors developed Nusselt number correlations for the PCM heat sink for different aspect ratios. Shatikian et al. [16] computationally studied the PCM behavior in a heat sink with vertical fins on its horizontal base. The PCM was stored between the fins, and a constant heat flux was applied at the horizontal base. Detailed parametric study was conducted. The thickness and height of the fins, thickness of the PCM layer, and heat flux varied. The transient behavior of the phase change was observed. The authors correlated the corresponding melt fractions and Nusselt numbers with Fourier, Stefan, and Rayleigh numbers. The current study aimed at analyzing the thermal performance of the microchannel PCM heat sink with salt hydrate S44 as the PCM [18]. The salt hydrate S44 is manufactured by PCM Products Ltd. in the form of standardized balls, tubes, and slabs stacked in underground or rooftop tanks for macroscale applications, such as refrigeration and free cooling, cryogenics, solar heating, heat

recovery, and industrial heating systems. The present study was aimed at acting as a feasibility study for production of S44 at the nanoscale for application in microchannel heat sinks by analyzing its performance through the computational method before its actual manufacturing.

For thermal performance analysis of the S44 slurries, the heat flux in the range of 8000 W/m^2 to 20,000 W/m^2 was applied. This range of heat flux values corresponds to the thermal dissipation characteristics of the fourth to the seventh generation of Intel® Core™ i3, i5, and i7 processors [19]. Each processor constitutes a 37.5 mm × 37.5 mm chip and dissipates 8.75 W to 32.50 W of thermal power for each independent CPU embedded inside the chip, thereby resulting in heat flux values ranging from 6222 W/m^2 to 23,111 W/m^2. The aim of the study was achieved by first analyzing the thermal performance of the salt hydrate S44 slurry in a microchannel PCM heat sink under different values of mass flow rate, heat flux, and concentration of the PCM. Then, we compared the thermal performance of the salt hydrate S44 with a similar study from the literature conducted for lauric acid nanoparticle slurry [11]. Finally, we developed Nusselt number correlations for the microchannel PCM heat sink to predict the thermal performance of the slurry using the Reynolds and Prandtl numbers of the fluid.

2. Methodology

Microchannel heat sinks are generally placed at the bottom of the printed circuit boards containing various electrical components on its surface. These electrical elements dissipate heat that must be removed from the circuit board. For this purpose, small-scale heat sinks are attached at the bottom to extract the heat with a circulating fluid. Figure 1(a) shows the schematic of a 3D model of a heat sink with a microchannel at the bottom. The electrical elements act as a source of constant heat flux. The 35 mm long microchannel possesses 2 mm × 50 μm cross section. Given that the aspect ratio (B/H) of the cross section is 40, the microchannel PCM heat sink can be considered as having a 2D geometry for the purpose of the investigation [9]. Figure 1(b) shows the schematic of the 2D computational domain used in the present study. Water-based salt hydrate S44 nanoparticle PCM slurry enters the microchannel through an inlet at a specified temperature and mass flow rate. Exchange of thermal energy occurs between the slurry and the top wall of the microchannel before the slurry exits the microchannel through the outlet at a higher temperature.

2.1. Mathematical Modelling and Thermophysical Properties of the Bulk Fluid. The salt hydrate S44 is a PCM produced at the macroscale by PCM Products, Ltd., in the PlusICE range [18]. The present research was a step toward the determination of the performance of salt hydrate S44 at the microscale by computationally developing the Nusselt number correlations when it is used as PCM to improve the cooling performance of microchannel heat sinks. The salt hydrate S44 slurry inside the microchannel was modeled as bulk fluid using the homogeneous approach. Table 1 presents the thermophysical properties of the homogeneous bulk fluid of S44 [18]. The literature suggests that the pressure drop can undergo significant deviation when the thermophysical properties remain constant with respect to temperature [11]. The pressure drop is an essential parameter that significantly contributes to the heat sink performance and helps determine the pumping requirement for the circulation of the cooling medium. Therefore, despite the expected longer computational time, the properties of the bulk fluid were assumed to be temperature dependent. The mathematical model of the PCM slurry flow inside the microchannel was a multiphysics model of fluid flow and heat transfer with phase change.

2.1.1. Fluid Flow Model. The conventional theory for continuum mechanics is applicable to the fluid flow inside microchannels with cross sections as small as 100 μm in width and 1.7 μm in height [20]. Therefore, Navier–Stokes equations can be used to model the flow inside the microchannel under consideration. The assumptions for the fluid flow model are as follows:

(i) The distribution of the particles is homogeneous throughout the microchannel [8]

(ii) The flow inside the microchannel is laminar and incompressible and at steady state [8]

(iii) The fluid is considered Newtonian below the 0.10 volumetric ratio concentration [8]

The governing equations for the flow of the PCM slurry are the following continuity and momentum equations [21]:

$$\frac{\partial u}{\partial x} + \frac{\partial u}{\partial y} = 0,$$

$$\rho_b\left(u\frac{\partial u}{\partial x} + v\frac{\partial u}{\partial y}\right) = -\frac{\partial p}{\partial x} + \mu_b\left(\frac{\partial^2 u}{\partial x^2} + \frac{\partial^2 u}{\partial y^2}\right), \quad (1)$$

$$\rho_b\left(u\frac{\partial v}{\partial x} + v\frac{\partial v}{\partial y}\right) = -\frac{\partial p}{\partial y} + \mu_b\left(\frac{\partial^2 v}{\partial x^2} + \frac{\partial^2 v}{\partial y^2}\right),$$

where u and v are the fluid velocities along the x and y directions, respectively, ρ_b represents the effective density of the bulk fluid, μ_b is the effective dynamic viscosity of the bulk fluid, and p is the pressure.

Effective density ρ_b of the PCM slurry is computed as the weighted average of the densities of the PCM nanoparticles and the carrier fluid [7], as follows:

$$\rho_b = C\rho_p + (1 - C)\rho_f, \quad (2)$$

where ρ_p and ρ_f are the densities of the PCM particle and the carrier fluid, respectively, and C is the PCM volumetric ratio concentration in the slurry.

Effective viscosity μ_b of the PCM slurry is computed using Vand's correlation [22], which was experimentally validated by Fang et al. in [23], as follows:

$$\mu_b = \left(1 - C - 1.16C^2\right)^{-2.5}\mu_f, \quad (3)$$

where μ_f is the dynamic viscosity of the carrier fluid.

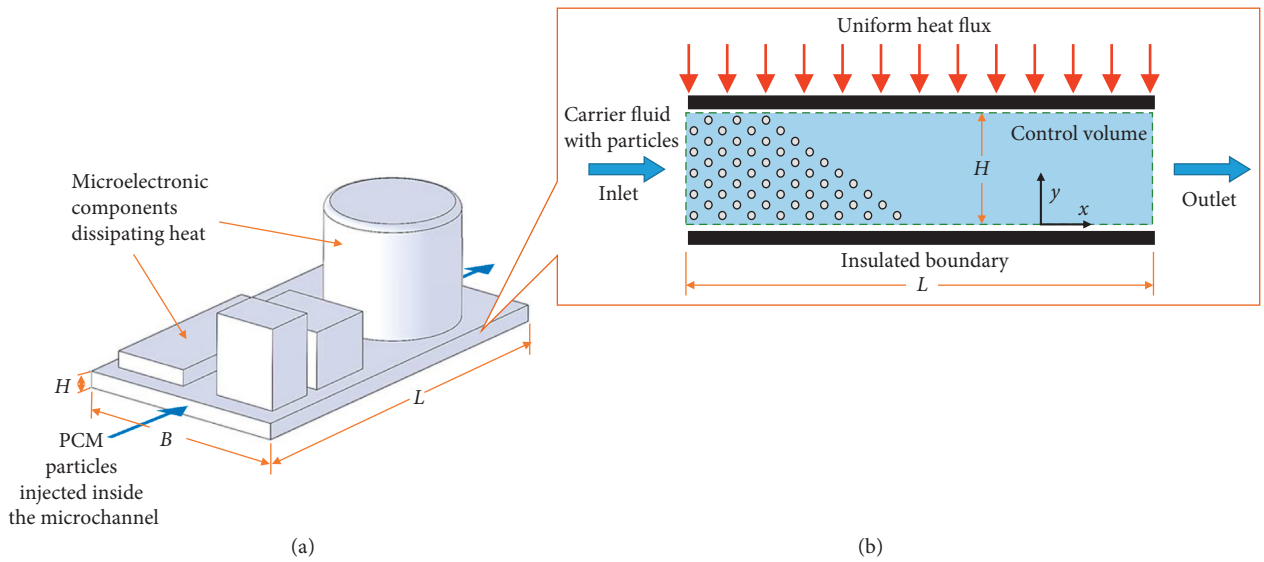

Figure 1: (a) 3D sketch of microchannel PCM heat sink and (b) 2D computational model.

Table 1: Thermophysical properties of the salt hydrate S44 [18].

PCM state	Density (kg/m^3)	Specific heat (kJ/kg·K)	Latent heat (kJ/kg)	Thermal conductivity (W/m·K)
Solid	1584	1.61	100	0.43
Liquid	—	1.61	—	0.43

2.1.2. Heat Transfer Model. Heat was transferred from the top wall where PCM changed its phase. The top wall had constant heat flux to the PCM slurry flowing through the microchannel. The physics of heat transfer with phase change was modeled using the energy equation of the convective heat transfer, assuming that the particles and the carrier fluid have the same velocity and temperature. Moreover, the thermophysical properties of the PCM slurry depend on the temperature. The 2D energy equation for the convection heat transfer [21] with negligible mechanical energy dissipation effects is as follows:

$$\rho_b c_b\left(u\frac{\partial T}{\partial x}+v\frac{\partial T}{\partial y}\right)=k_b\left(\frac{\partial^2 T}{\partial x^2}+\frac{\partial^2 T}{\partial y^2}\right), \tag{4}$$

where T represents the temperature distribution in the microchannel and u and v are the velocity components along the x and y axes, respectively. ρ_b and c_b are the density and specific heat of the bulk fluid, respectively. k_b is the effective thermal conductivity of the PCM slurry and a combination of the thermal conductivity of the particles k_p and carrier fluid k_f. k_b can be computed using Maxwell's relation [24], as follows:

$$k_b=k_f\frac{2+\left(k_p/k_f\right)+2C\left(\left(k_p/k_f\right)-1\right)}{2+\left(k_p/k_f\right)-C\left(\left(k_p/k_f\right)-1\right)}, \tag{5}$$

where C is the PCM volumetric ratio concentration in the slurry.

2.1.3. Phase Change Model. Heat was transferred from the top surface of the microchannel to the carrier fluid containing nanoparticles. These particles instantaneously melted to form a PCM slurry when the melting temperature is reached. During the phase change process, heat was stored in the PCM. The heat storage capacity of the PCM slurry can be determined by conducting an energy balance of the phase change process [7]. The energy balance model required the assumption of a piecewise function of specific heat correlation broken at the solidus and liquidus temperatures, which may be located with a difference of 0.5 K in either direction of the PCM melting temperature. The bulk fluid specific heat c_b can be modeled in various ways, depending on the particle temperature relative to the temperatures of the solidus and liquidus regions of the slurry. If the particle temperature was less than the solidus temperature, c_b was computed as follows:

$$c_b=\frac{C\rho_p c_{S,p}+(1-C)\rho_f c_f}{\rho_b}. \tag{6}$$

In case the temperature of the particles was greater than the solidus temperature but less than the liquidus temperature, c_b was modelled as a function of the specific heats of the solidus ($c_{S,p}$) and liquidus phases ($c_{L,p}$) and latent heat of fusion L_{fusion}, as follows:

$$c_b=\frac{C\left(c_{S,p}+c_{L,p}\right)}{2}+\frac{CL_{fusion}}{T_{liquidus}-T_{solidus}}+\frac{(1-C)\rho_f c_f}{\rho_b}. \tag{7}$$

When the temperature of particle exceeded that of the liquidus phase, the correlation of the specific heat was as follows:

$$c_b=\frac{C\rho_p c_{L,p}+(1-C)\rho_f c_f}{\rho_b}. \tag{8}$$

3. Implementation of the Numerical Method

The mathematical model developed in the previous section was translated into a computational model for implementation. Discretization of the governing equations was conducted using the finite volume approach in ANSYS Fluent (V 16.1) [17]. All variables in the numerical solution were computed at each node, except for the velocities computed midway between the nodes. The pressure-based segregated algorithm, known as SIMPLE, was used to achieve pressure-velocity coupling in the governing equations [25]. Residuals were carefully monitored with convergence criteria of 10^{-9} for the continuity and momentum equations and 10^{-12} for the energy equation. Additionally, convergence was ensured by monitoring the temperature at the outlet throughout the simulations.

3.1. Mesh Properties and Mesh Independence Study. A staggered 2D grid consisting of rectangular and triangular elements was used in the study. A fine mesh was kept near the top and bottom regions to accurately capture the flow property gradients normal to the flow direction. Mesh independence study was conducted by computing local Nusselt numbers along the length of the microchannel for the grid resolutions of 8 × 5600, 10 × 7000, and 12 × 8400 as shown in Figure 2. The maximum difference between the Nusselt numbers for different grid resolutions was 0.086. Therefore, the grid resolution of 10 × 7000 was used in further simulations.

3.2. Model Validation. The computational model was compared with that of the experimental study of Goel et al. [2]. A model with a circular channel that is 3.14 mm in diameter was considered to possess a wall temperature profile. The same experimental conditions, such as Reynolds number of 200, Stefan number of 2, and PCM volumetric ratio concentration of 0.10, were used for the comparison. Comparison between experimental and computational values of the wall temperature along the microchannel has been shown in Figure 3. Evidently, both studies are in agreement with a 1.23% maximum percentage difference between the two temperatures.

4. Results and Discussion

The developed numerical model was simulated using ANSYS Fluent (V. 16.1) [17]. Results were postprocessed to obtain the performance parameters and development of the Nusselt number correlations.

4.1. Thermal Performance Evaluation of Salt Hydrate S44. Heat flux and mass flow rate were varied to investigate the performance of the microchannel heat sink. Given that both parameters are critical to the heat transfer, the combined effects on the three performance parameters—effectiveness ratio, performance index, and Merit number—were obtained in the form of heat flux to mass flow rate ratio.

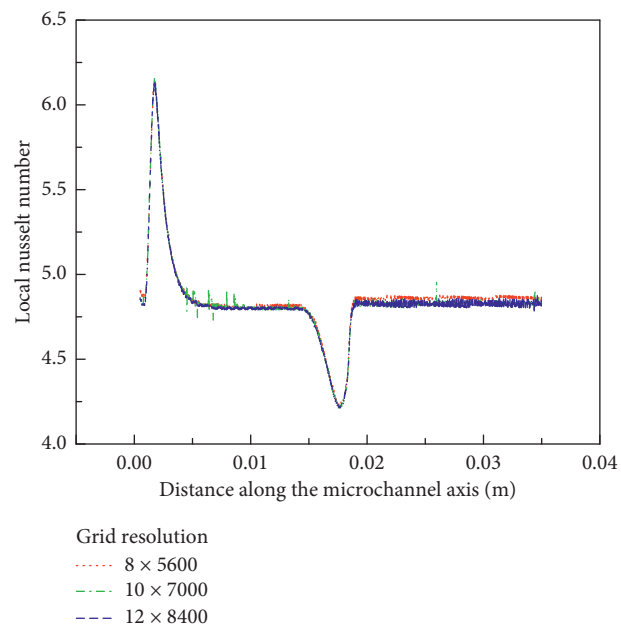

Figure 2: Local Nusselt number variations along the microchannel axis for different mesh resolutions.

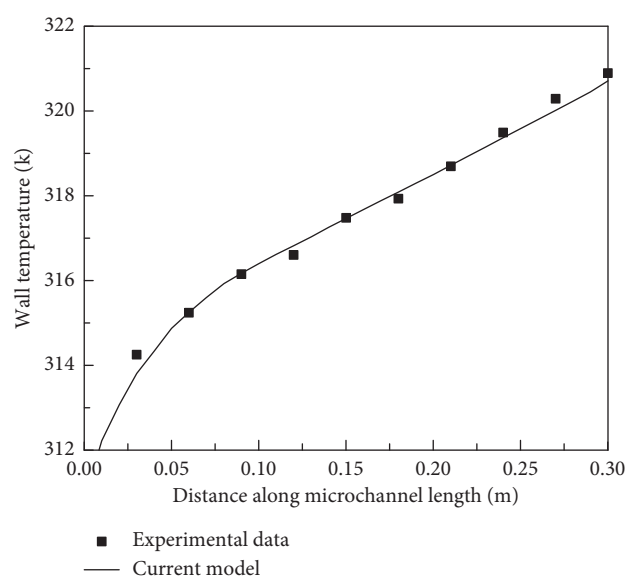

Figure 3: Validation of the computational model against experimental data [2].

4.1.1. Effectiveness Ratio. Effectiveness ratio is a measure of the heat transfer enhancement caused by the addition of the PCM nanoparticles to the carrier fluid [1]. It can be quantified as the ratio of the rate of heat transfer of bulk fluid and the rate of heat transfer of the carrier fluid. It is given as follows:

$$\varepsilon_{\text{eff}} = \frac{Q_b}{Q_f}, \tag{9}$$

where Q_b and Q_f are the heat transfer rates of the bulk fluid and the carrier fluid, respectively. They are calculated as follows:

$$Q_b = q'' \times A,$$
$$Q_f = \dot{m} c_f \Delta T, \quad (10)$$

where q'' is the top wall heat flux in W/m^2, A is the area of the top wall in m^2, $\dot{m}$ is the mass flow rate in kg/s, c_f is the specific heat of the carrier fluid in J/kg·K, and ΔT is the temperature rise along the microchannel length in Kelvin.

Figure 4 shows the effect of heat flux per unit mass flow rate of the bulk fluid for various concentrations of the salt hydrate S44 on the effectiveness ratio. When the particles started melting in the microchannel, the effectiveness ratio reached the maximum value because of the highest ratio of sensible heat to latent heat of the bulk fluid. For this peak value of the effectiveness ratio, the largest length was that along which the particles melt inside the microchannel. Given that the sensible heat region near the inlet of the microchannel cannot be avoided, the maximum value of the effectiveness ratio corresponded to the circumstance when the sensible heat region at the inlet was minimized, and the remaining distance inside the microchannel was covered by the latent heat region. This configuration ensured minimal temperature increase between the inlet and the outlet regions of the microchannel. Hence, for a given concentration of the PCM, an optimal ratio of the heat flux to mass flow rate existed in a region where the largest amount of heat transfer occurred for minimum temperature increase along the heat sink. Consequently, a value below this optimal value indicated that the particles were not completely melted inside the microchannel. Moreover, this optimal value minimized the sensible region near the inlet, and the particles melted just before the outlet. However, a heat flux per unit mass flow rate above the optimal value showed that the particles melted earlier on the inside of the microchannel. A region of sensible heat was left at the end of the microchannel, thereby indicating a nonoptimised design of the microchannel under the given operating conditions. Furthermore, the plot of effectiveness ratio for bulk fluid containing lauric acid as the PCM nanoparticle was presented in Figure 5 for a performance comparison between lauric acid and S44. It is suggested that the slurry with lauric is able to absorb slightly more heat dissipated from the electronic components in comparison with S44.

4.1.2. Performance Index. Performance index is defined as the ratio of the heat transfer rate per unit pumping power of the bulk fluid to the heat transfer rate per unit pumping power of the carrier fluid [1]. The performance index helps the manufacturer in deciding the amount of pumping power and is given as follows:

$$\text{performance index} = \frac{(Q_b/P_b)}{(Q_f/P_f)}, \quad (11)$$

where P_b and P_f are the pumping powers of the bulk and the carrier fluid, respectively, and can be computed as follows:

$$P_b = \Delta p_b u_b A,$$
$$P_f = \Delta p_f u_f A, \quad (12)$$

where Δp_b and Δp_f are the pressure drops in case of the bulk and the carrier fluid, respectively, in atm; A is the top wall area in m^2; and u_b and u_f are the velocities of the bulk and the carrier fluid, respectively, in m/s. The pressure drop of the carrier fluid can be computed using the Reynolds number Re_f calculated based on the hydraulic diameter D_h of the microchannel, as follows:

$$\Delta p_f = \frac{32 L \rho_f u_f^2}{\mathrm{Re}_f D_h},$$
$$\mathrm{Re}_f = \frac{\rho_f u_f D_h}{\mu_f}, \quad (13)$$

where ρ_f is the density of the carrier fluid in kg/m^3, L is the microchannel length in meters, and μ_f is the dynamic viscosity of the carrier fluid in Pa·s.

Figure 6 shows the effect of the heat flux per unit mass flow rate on the performance index for various concentrations of

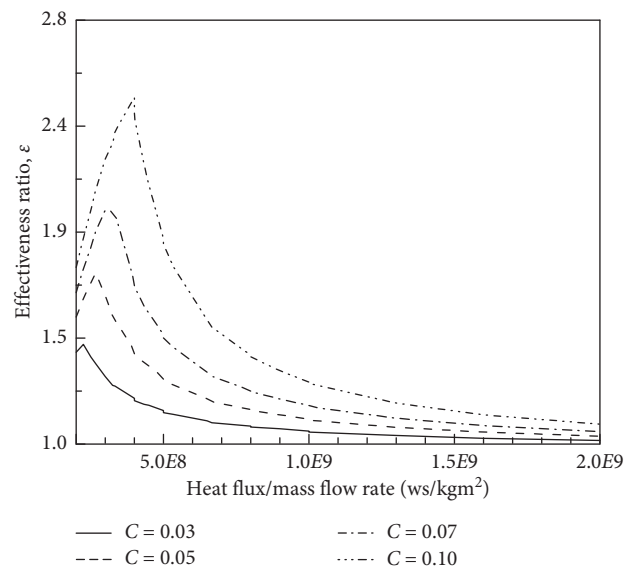

Figure 4: Effect of heat flux per unit mass flow rate on the effectiveness ratio at various concentrations of S44 PCM slurry.

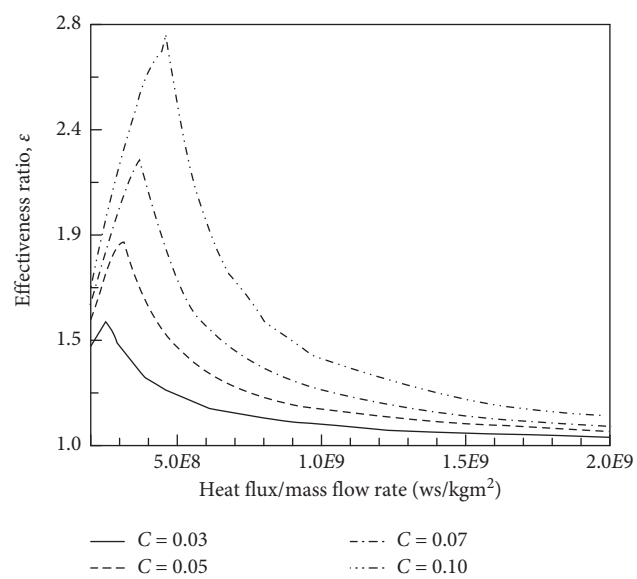

Figure 5: Effect of heat flux per unit mass flow rate on the effectiveness ratio for various concentrations of lauric acid slurry [11].

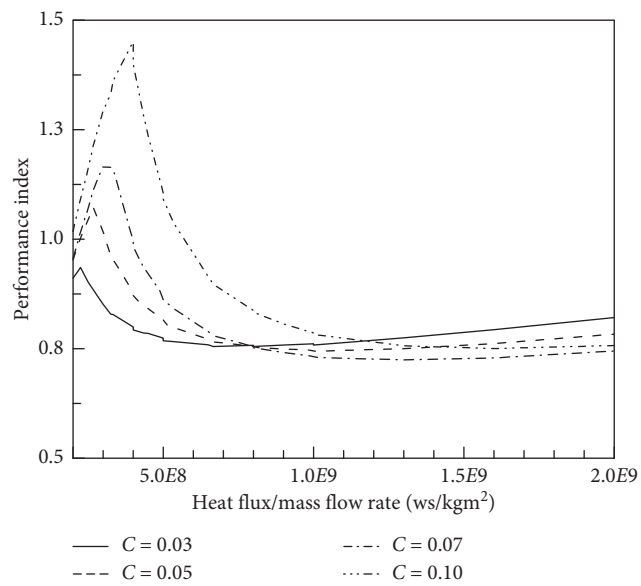

Figure 6: Effect of heat flux per unit mass flow rate on the performance index for various concentrations of S44 PCM slurry.

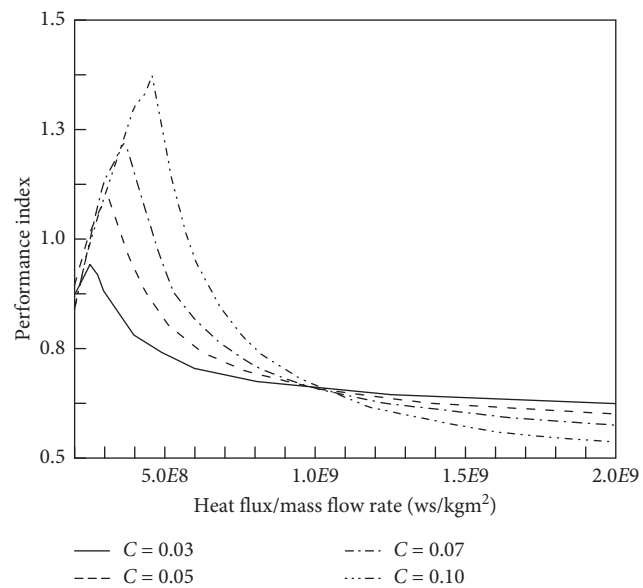

Figure 7: Effect of heat flux per unit mass flow rate on the performance index for various concentrations of lauric acid slurry [11].

S44. The performance index exhibited a similar pattern when the heat flux to mass flow rate ratio is increased. However, the fluid with smaller particle concentration performs better than those with higher concentration for higher heat flux per unit mass flow rate values. This anomaly in the trend indicated the effect of pressure drop caused by the larger concentrations of S44 in the carrier fluid, and a new expression for the performance index was considered, as follows:

$$\text{performance index} = \frac{\varepsilon_{\text{eff}}}{\Delta p_{\text{b}}} \times \frac{P_{\text{f}}}{u_{\text{b}} A}. \tag{14}$$

This expression shows the direct relationship between performance index and effectiveness ratio. However, the performance index was inversely related to the pressure drop along the microchannel. The increase in pressure drop with increase in the heat flux to mass flow rate ratio may be attributed to the decrease in the temperature gradient along the length of the microchannel with increasing PCM concentration. Vand's correlation, as given in equation (3), shows that the viscosity decreases with rise in temperature. Therefore, at a higher value of heat flux per unit mass flow rate, a lower rate of increase in the effectiveness ratio with respect to the increase in PCM concentration resulted in higher temperature increase rate, thereby decreasing viscosity at a high rate and resulting in a higher increase of pressure drop rate. At higher values of heat flux per unit mass flow rate, the rate of increase in the effectiveness ratio with respect to the PCM concentration was lower than the rate of increase of the pressure drop. Therefore, as predicted by equation (14), the performance index was lower for higher PCM concentrations at higher values of heat flux per unit mass flow rate. Figure 7 provides the performance index plot of the bulk fluid containing lauric acid as PCM. The comparison clearly showed that the heat transfer rate per fluid pumping power of S44 is higher than that of the lauric acid slurry flow for the considered operating conditions. Hence, S44 provided more practical option as a PCM slurry selection for the objectives of this study.

4.1.3. Merit Number. Merit number is the measure of the irreversibility of the heat transfer and frictional losses because of the addition of PCM nanoparticles. It is defined as the ratio of the gain in heat transfer due to the process of addition of PCM particles to the sum of heat transferred at the top wall of the microchannel and the irreversibility [11]. Such irreversibility can be the reason for using the volumetric entropy generation rate S''_{gen} (in W/m^3·K), as follows:

$$S'''_{\text{gen}} = \frac{k_{\text{b}}}{T^2}\left[\left(\frac{\partial T}{\partial x}\right)^2 + \left(\frac{\partial T}{\partial y}\right)^2\right] + \frac{\mu_{\text{b}}}{T}\left(\frac{\partial u}{\partial y}\right)^2, \tag{15}$$

where k_{b} is the thermal conductivity of the bulk fluid in W/m·K and μ_{b} is the dynamic viscosity bulk fluid in Pa·s.

Hence, the Merit number is given as follows:

$$M = \frac{Q_{\text{gain}}}{Q_{\text{b}} + \dot{I}}, \tag{16}$$

where Q_{gain} is the gain rate of heat absorption into the slurry due to addition of the particles (W) and $\dot{I}$ is the rate of irreversibility (W). It can be computed as follows:

$$\begin{aligned} Q_{\text{gain}} &= Q_{\text{b}} - Q_{\text{f}} = Q_{\text{f}}\left(\varepsilon_{\text{eff}} - 1\right), \\ \dot{I} &= S'''_{\text{gen,avg}} \times \text{volume} \times T_{\text{ref}}, \end{aligned} \tag{17}$$

where the reference temperature T_{ref} is maintained at 298 K.

Figure 8 shows the effect of heat flux per unit mass flow rate on the Merit number for various concentrations of S44 in the bulk fluid. Merit number also shows a similar trend with increasing heat flux per unit mass flow rate as in the previous cases of effectiveness ratio and performance index. However, the increase in concentration reduced the irreversibility, demonstrating the improvement in heat transfer. The increasing heat flux per unit mass flow rate hinted at the increase in irreversibility. In an adverse situation, this trend of continuous decrease in the Merit number may lead to zero. Therefore, a reasonable heat flux per unit mass flow

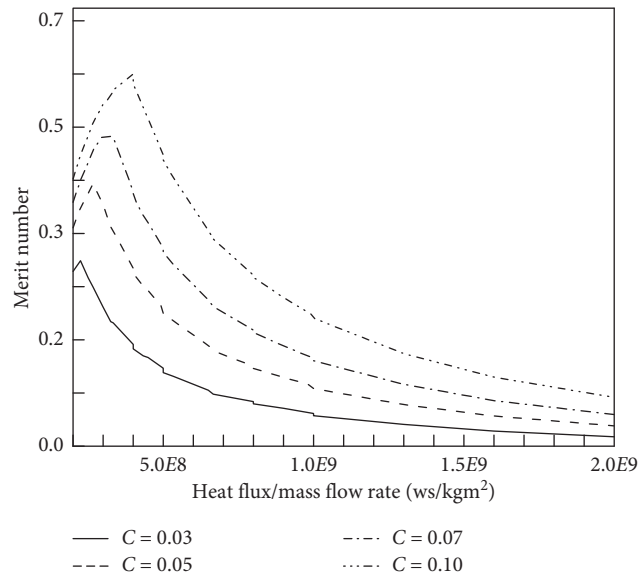

Figure 8: Effect of heat flux per unit mass flow rate on the Merit number for various concentrations of S44 slurry.

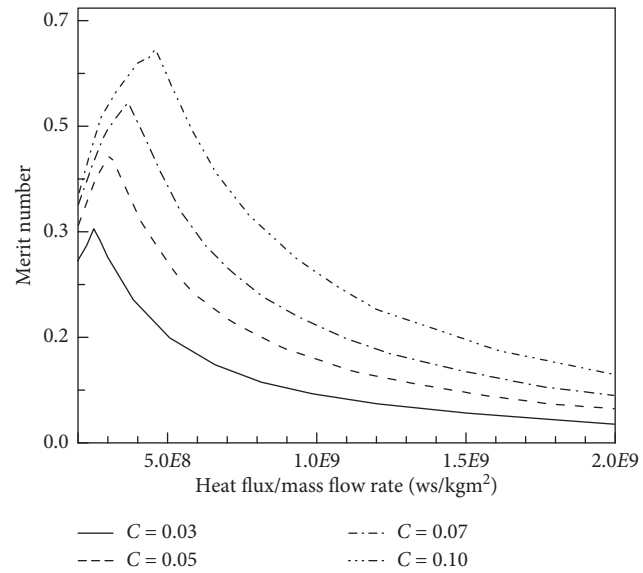

Figure 9: Effect of heat flux per unit mass flow rate on the Merit number for various concentrations of lauric acid slurry [11].

rate combination must be adopted to minimize irreversibility, especially with increasing PCM concentration. A comparison between the Merit number of lauric acid and S44 under the same conditions suggests that the lauric acid slurry offers marginally less losses than the S44 slurry at the same concentration (Figure 9).

4.2. Development of Nusselt Number Correlations. Any problem of convection is essentially a problem of computing the heat transfer coefficient [21]. Nusselt number $\overline{\mathrm{Nu}}_{\mathrm{L}}$ is the nondimensionalized form of the heat transfer coefficient and may be correlated with Reynolds number Re and the Prandtl number Pr of the convective fluid flow by equations of the form $\overline{\mathrm{Nu}}_{\mathrm{L}} = f(\mathrm{Re}, \mathrm{Pr})$. In order to obtain the Nusselt number correlations for the microchannel PCM heat sink, the data from the study were correlated in terms of averaged Nusselt, Reynolds, and Prandtl numbers.

To develop the Nusselt number correlations for the PCM heat sink, sets of Prandtl number, Reynolds number, and Nusselt number for the convective flow inside the microchannel were obtained, corresponding to each individual operating condition. The Prandtl numbers ranged from 3.74 to 5.30, whereas the wall temperatures ranged between 316.5 and 332.4 K for the PCM concentrations under study. Each data point on the plot represents a unique set of operating conditions for the heat sink. The average Nusselt number was plotted against the average Reynolds number on the log-log scale as shown in Figure 10. The form of the plot obtained hints at the need for Prandtl number normalization. Therefore, the $\overline{\mathrm{Nu}}_{\mathrm{L}}$ data set was normalized by the Prandtl number to the power 0.8 in order to obtain a linear assortment of the data points (Figure 11). The power law dependence was strictly suggested by this plot.

By inspection, each separate line in the plot shown in Figure 11 represents each of the four values of mass flow rates considered in this study. The four power laws thus

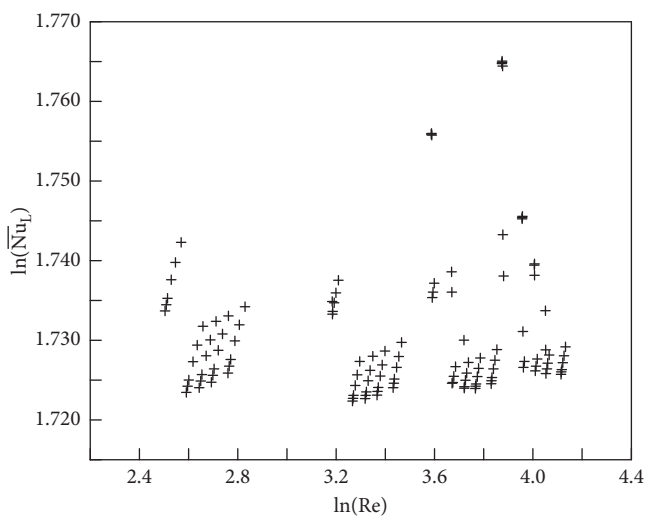

Figure 10: Average Nusselt number plotted against average Reynolds number of the slurry flow on the log-log scale.

obtained are the Nusselt number correlations listed in Table 2 along with the corresponding convective heat transfer coefficients for the microchannel PCM heat sink under study. In Table 2, $\overline{\mathrm{Nu}}_{\mathrm{L}}$ represents the average Nusselt number, h represents the convective heat transfer coefficient in W/m^2-K, Re represents the Reynolds number, and Pr represents the Prandtl number. The developed convective heat transfer coefficient equations for the microchannel PCM heat sink prediction accuracies were 2.71%, 3.17%, 2.52%, and 3.20% for each range of the Reynolds number.

5. Conclusion

The thermal performance of the water-based salt hydrate S44 slurry flow through a microchannel heat sink was analyzed.

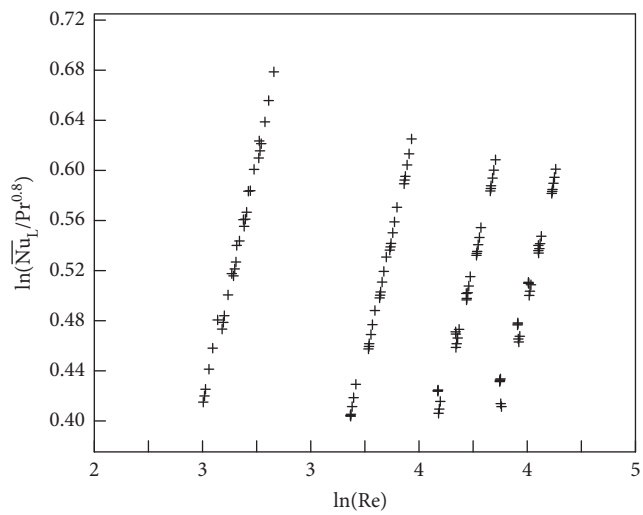

Figure 11: Average Nusselt number normalized by the Prandtl number to the power 0.8.

Table 2: Correlations for average Nusselt number and convective heat transfer coefficient for the microchannel PCM heat sink.

Range of the Reynolds number	$\overline{\mathrm{Nu}}_{\mathrm{L}} = A\,\mathrm{Re}^{B}\mathrm{Pr}^{C}$	$h = D\,\mathrm{Re}^{E}\mathrm{Pr}^{F}$ (W/m^2·K)
$12.23 < \mathrm{Re} < 16.94$	$\overline{\mathrm{Nu}}_{\mathrm{L}} = 0.213\,\mathrm{Re}^{0.783}\mathrm{Pr}^{0.800}$	$h = 1380\,\mathrm{Re}^{0.783}\mathrm{Pr}^{0.800}$
$24.13 < \mathrm{Re} < 32.00$	$\overline{\mathrm{Nu}}_{\mathrm{L}} = 0.133\,\mathrm{Re}^{0.761}\mathrm{Pr}^{0.800}$	$h = 856\,\mathrm{Re}^{0.761}\mathrm{Pr}^{0.800}$
$36.12 < \mathrm{Re} < 47.14$	$\overline{\mathrm{Nu}}_{\mathrm{L}} = 0.116\,\mathrm{Re}^{0.713}\mathrm{Pr}^{0.800}$	$h = 745\,\mathrm{Re}^{0.713}\mathrm{Pr}^{0.800}$
$48.11 < \mathrm{Re} < 62.29$	$\overline{\mathrm{Nu}}_{\mathrm{L}} = 0.114\,\mathrm{Re}^{0.668}\mathrm{Pr}^{0.800}$	$h = 731\,\mathrm{Re}^{0.668}\mathrm{Pr}^{0.800}$

Pr: Prandtl number, such that $3.74 < \mathrm{Pr} < 5$; q'': the top plate heat flux, such that 8000 W/m^2 $< q'' <$ 20,000 W/m^2; T_{w}: wall temperature, such that 316.5 K $< T_{\mathrm{w}} <$ 332.4 K.

Three performance parameters, namely, effectiveness ratio, performance index, and Merit number, were utilized to quantify the cooling performance of S44 for various concentrations of the PCM nanoparticles. A combined effect of heat flux and mass flow rate was examined in the form of heat flux per unit mass flow rate. Moreover, Nusselt number correlations were developed as a function of Reynolds and Prandtl numbers under a range of operating conditions.

The effectiveness ratio attained its peak value when the phase change region inside the microchannel was maximized. This configuration corresponded to the minimum temperature rise, thereby not only allowing maximum heat transfer to occur from the electronic component to the heat sink but also reducing the unnecessary thermal expansions that can damage the electronic component. Performance index helped the manufacturer determine the pumping power requirement based on the increase of pressure drop with increasing PCM concentration that was required for the electronic component for which the heat sink is to be designed. Given the heat flux of the electronic component, a mass flow rate for the slurry was set, thereby minimizing the power required to pump the slurry through the microchannel. A comparative analysis of the salt hydrate S44 with lauric acid showed that the latter slurry absorbed more heat flux than the former under the investigated operating conditions; however, this occurred at the cost of higher pumping power requirement. The losses due to the addition of the PCM particles were only marginally less in lauric acid than in S44 at the same concentration.

Nomenclature

A: Microchannel cross-sectional area (m^2)
C: Volumetric ratio concentration of PCM nanoparticles
c_{p}: Isobaric specific heat (J·kg^{-1}·K^{-1})
$c_{\mathrm{p,L}}$: Isobaric specific heat of the PCM particles in the solid state (J·kg^{-1}·K^{-1})
$c_{\mathrm{p,S}}$: Isobaric specific heat of the PCM particles in the liquid state (J·kg^{-1}·K^{-1})
$\overline{\mathrm{Nu}}_x$: Average Nusselt number over the interval $(0, x)$
D_{h}: Hydraulic diameter (m)
$\dot{I}$: Irreversibility rate (W)
h: Convective heat transfer coefficient (W·m^{-2}·K^{-1})
k: Thermal conductivity (W·m^{-1}·K^{-1})
L: Microchannel length (m)
L_{fusion}: Latent heat of fusion (J·kg^{-1})
$\dot{m}$: Mass flow rate of PCM slurry (kg·s^{-1})
P: Pumping power (W)
p: Pressure (Pa)
Q: Rate of heat transfer (W)
q'': Heat flux (W·m^{-2})
S'': Volumetric entropy generation rate (W·m^{-3}·K^{-1})
T: Temperature (K)
T_{in}: Inlet temperature (K)
T_{out}: Outlet temperature (K)
T_{w}: Wall temperature (K)
T_{liquius}: Liquidus temperature (K)
T_{solidus}: Solidus temperature (K)

u: Velocity along the x axis ($m \cdot s^{-1}$)
v: Velocity along the y axis ($m \cdot s^{-1}$)
ρ: Density ($kg \cdot m^{-3}$)
μ: Dynamic viscosity (Pa·s).
Subscripts
b: Bulk fluid
f: Carrier fluid
p: Particle.

Data Availability

The data used to support the findings of this study are included within the article.

Conflicts of Interest

The authors declare that they have no conflicts of interest.

Acknowledgments

This study was supported by the National Research Foundation of Korea (NRF), which is a grant funded by the Korea government (MSIP) (no. 2017R1A2B2005515).

References

[1] K. Q. Xing, Y.-X. Tao, and Y. L. Hao, "Performance evaluation of liquid flow with PCM particles in microchannels," *Journal of Heat Transfer*, vol. 127, no. 8, pp. 931–940, 2005.
[2] M. Goel, S. K. Roy, and S. Sengupta, "Laminar forced convection heat transfer in microcapsulated phase change material suspensions," *International Journal of Heat and Mass Transfer*, vol. 37, no. 4, pp. 593–604, 1994.
[3] S. K. Roy and S. Sengupta, "An evaluation of phase change microcapsules for use in enhanced heat transfer fluids," *International Communications in Heat and Mass Transfer*, vol. 18, no. 4, pp. 495–507, 1991.
[4] J. L. Alvarado, C. Marsh, C. Sohn, G. Phetteplace, and T. Newell, "Thermal performance of microencapsulated phase change material slurry in turbulent flow under constant heat flux," *International Journal of Heat and Mass Transfer*, vol. 50, no. 9-10, pp. 1938–1952, 2007.
[5] Y. L. Hao and Y. X. Tao, "A numerical model for phase-change suspension flow in microchannels," *Numerical Heat Transfer, Part A: Applications*, vol. 46, no. 1, pp. 55–77, 2004.
[6] S. Kuravi, J. Du, and L. C. Chow, "Encapsulated phase change material slurry flow in manifold microchannels," *Journal of Thermophysics and Heat Transfer*, vol. 24, no. 2, pp. 364–373, 2010.
[7] R. Sabbah, M. M. Farid, and S. Al-Hallaj, "Micro-Channel Heat sink with slurry of water with micro-encapsulated phase change material: 3d-numerical study," *Applied Thermal Engineering*, vol. 29, no. 2-3, pp. 445–454, 2009.
[8] S. Kuravi, K. M. Kota, J. Du, and L. C. Chow, "Numerical investigation of flow and heat transfer performance of nano-encapsulated phase change material slurry in microchannels," *Journal of Heat Transfer*, vol. 131, no. 6, article 062901, 2009.
[9] S. Kondle, J. L. Alvarado, and C. Marsh, "Laminar flow forced convection heat transfer behavior of a phase change material fluid in microchannels," *Journal of Heat Transfer*, vol. 135, no. 5, article 052801, 2013.
[10] A. B. S. Alquaity, S. A. Al-Dini, E. N. Wang, S. Z. Shuja, B. S. Yilbas, and K. J. Suabedissen, "Heat transfer enhancement in microchannel flow: presence of microparticles in a fluid," in *Proceedings of ASME 2010 8th International Conference on Nanochannels, Microchannels, and Minichannels: Parts A and B*, pp. 353–358, Montreal, QC, Canada, August 2010.
[11] A. B. S. Alquaity, S. A. Al-Dini, E. N. Wang, and B. S. Yilbas, "Numerical investigation of liquid flow with phase change nanoparticles in microchannels," *International Journal of Heat and Fluid Flow*, vol. 38, pp. 159–167, 2012.
[12] A. B. S. Alquaity, S. A. Al-Dini, and B. S. Yilbas, "Investigation into thermal performance of nanosized phase change material (PCM) in microchannel flow," *International Journal of Numerical Methods for Heat & Fluid Flow*, vol. 23, no. 2, pp. 233–247, 2013.
[13] U. Stritih, "An experimental study of enhanced heat transfer in rectangular PCM thermal storage," *International Journal of Heat and Mass Transfer*, vol. 47, no. 12-13, pp. 2841–2847, 2004.
[14] X. Wang, J. Niu, Y. Li et al., "Heat transfer of micro-encapsulated PCM slurry flow in a circular tube," *AIChE Journal*, vol. 54, no. 4, pp. 1110–1120, 2008.
[15] S. K. Saha and P. Dutta, "Heat transfer correlations for PCM-based heat sinks with plate fins," *Applied Thermal Engineering*, vol. 30, no. 16, pp. 2485–2491, 2010.
[16] V. Shatikian, G. Ziskind, and R. Letan, "Numerical investigation of a PCM-based heat sink with internal fins: constant heat flux," *International Journal of Heat and Mass Transfer*, vol. 51, no. 5-6, pp. 1488–1493, 2008.
[17] ANSYS, *ANSYS FLUENT Theory Guide*, ANSYS, Inc., Canonsburg, PA, USA, 2010.
[18] PCM Products Ltd., *PlusICE—Phase Change Materials*, PCM Products Ltd., Yaxley, UK, 2013.
[19] Intel ® product specifications," September 2018, http://ark.intel.com/.
[20] S. G. Kandlikar and W. J. Grande, "Evolution of microchannel flow passage thermohydraulic performance and fabrication technology," *Heat Transfer Engineering*, vol. 24, no. 1, pp. 3–17, 2003.
[21] P. I. Frank, D. Bergan, and A. Lavine, *Fundamentals of Heat and Mass Transfer*, John Wiley & Sons, Jefferson City, MO, USA, 2007.
[22] V. Vand, "Theory of viscosity of concentrated suspensions," *Nature*, vol. 155, no. 3934, pp. 364-365, 1945.
[23] Y. Fang, S. Kuang, X. Gao, and Z. Zhang, "Preparation of nanoencapsulated phase change material as latent functionally thermal fluid," *Journal of Physics D: Applied Physics*, vol. 42, no. 3, article 0305407, 2009.
[24] J. Maxwell, *A Treatise on Electricity and Magnetism*, Dover Publications, New York, USA, 2008.
[25] S. V. Patankar, *Numerical Heat Transfer and Fluid Flow*, Taylor & Francis Group, New York, USA, 1980.